

Design and control of a grid-connected solar-wind hybrid sustainable energy generation systems using DFIG

G. B. Arjun Kumar¹, M. Balamurugan¹, K. N. Sunil Kumar², Ravi Gatti³

¹Department of Electrical and Electronics Engineering, Dayananda Sagar College of Engineering, Bengaluru, India

²Department of Information Science and Engineering, Sri Venkateshwara College of Engineering, Bengaluru, India

³Department of Electronics and Communication Engineering, Dayananda Sagar Academy of Technology and Management, Bengaluru, India

Article Info

Article history:

Received Feb 18, 2024

Revised Sep 23, 2024

Accepted Oct 23, 2024

Keywords:

DFIG

Grid side converter

Maximum power point tracking

Optimal torque

Perturb and observe

Photovoltaic

Rotor side converter

ABSTRACT

An optimal control of a grid-connected solar-wind hybrid scheme for the electricity generation system by utilizing both wind and solar renewable energy in a remote region that is inaccessible to the electricity grid. The control and assessment of a hybrid sustainable energy generation system power system that supplies three-phase, four-line loads as well as a battery array are presented in this research work. Wind energy conversion system (WECS) is comprised of a doubly-fed induction generator (DFIG) and two pulse width modulation (PWM) voltage source converters, namely the grid side converter (GSC) and the rotor side converter (RSC), which are linked together via a DC-link and are equipped with a technique for maximum power point tracking (MPPT). The grid voltage-oriented control strategy is employed to provide a consistent DC-bus voltage for the GSC and to regulate the reactive power on the power grid. Even the difference in voltage and frequency can be controlled with this novel strategy. The stator voltage-oriented vector technique is designed in the RSC control strategy, resulting in effective regulation of reactive and active power at the stator as well as an MPPT obtained by controlling the optimal torque. The hybrid sustainable energy generating system (HSEGS) simulation model is designed to have a capacity of 5 kW, and its efficiency is evaluated using the MATLAB/Simulink platform and demonstrated in a variety of circumstances.

This is an open access article under the [CC BY-SA](#) license.



Corresponding Author:

G. B. Arjun Kumar

Department of Electrical and Electronics Engineering, Dayananda Sagar College of Engineering
Bengaluru, Karnataka 560078, India

Email: arjun-eee@dayanandasagar.edu

1. INTRODUCTION

Since electrical energy has become a necessity in today's world, where nearly every area of human activity is governed by some type of advanced technology. According to recent research on India's 19th Electric Power Survey, the maximum electricity demand in 2030–2031 would be 600 GW, and in 2048–2050, it would be 1200 GW [1]. To fulfil this ever-demanding electrical energy, it is essential to utilise all the available renewable sources of energy, whether to enhance grid power or to provide isolated loads. By 2021, global renewable energy capacity will reach 2799 GW, with hydropower continuing to contribute the biggest portion (1211 GW), while renewable energy is coming up quickly. Renewable energy sources are being implemented not only to replace dwindling fossil fuels but also to minimise environmental contamination and contribute to the creation of an eco-friendly system [2].

The worldwide wind energy and solar energy scenario in our country (India) plays a part in our outstanding performance as well. By the end of February 29, 2020, India will have reached fourth place in the world, having installed 86.76 GW of grid-connected renewable energy, of which 37.6 GW comes from wind energy. India, which was ranked tenth on the chart five years ago, increased its capacity to about 40 GW in 2020, jumping to fifth place. According to India's National Institute of Wind Energy, the nation has a wind capacity of around 651 GW at a hub height of 100m and a solar potential of over 750 GW, provided that unused land is readily accessible [3]. The Indian government recently established a programme called the "Deen Dayal Upadhyaya Gram Jyoti Yojana" with the vision of attaining 100% rural electricity. Thus, it is expected that power generation using sustainable energy sources like solar and wind energy will result in not only ecologically friendly electricity generation but also in meeting the electricity demands of those living in remote areas [4].

Continuous investigations into the evolution of wind turbines (WTs) have resulted in a continuous rise in wind turbine capacities, from 50 kW in the mid-1980s to the current 9.5 MW capacity of WTs. Thus, with such advancements in technology, wind energy generation is almost comparable with traditional sources of electricity. Electricity generated by the huge capacity of WTs is used to deliver power directly to the grid. For stand-alone power deliveries, smaller turbines in the 100-kW range with appropriate power electronic controllers are explored. Additionally, apart from large-scale grid-connected solar farms, the development of small solar-driven off-grid installations seems to have been spectacular globally, with India leading the way with an estimated 5,544 such off-grid systems deployed in 2020. In light of the above discussion, a novel hybrid method for powering isolated loads using solar and wind energy has been suggested [5], [6].

To generate electricity from wind, adequate electrical generators are necessary during the energy conversion at the initial stage. In comparison to any other type of electrical generator, the doubly fed induction generator (DFIG) may be configured to produce a constant frequency and voltage at the stator, irrespective of the rotor speed or load [7]. Additionally, DFIGs work across a wide range of speeds and require lower power converter ratings. Traditionally, it has been suggested that it operates via a back-to-back (BTB)-linked converter arrangement. DC links are widely utilized in BTB topologies; therefore, the regulation of converters is interlinked. The second power converter is needed at the DC link to accommodate the energy storage system (ESS) used to control the changing wind speed. To minimize the number of power converters while integrating an ESS, a combined inverter-battery configuration is suggested for grid-connected and stand-alone functioning of DFIG [8]. This arrangement is capable of supplying isolated loads with a fixed frequency and voltage magnitude, regardless of the rotational velocity or load. Thus, to maximize the simplicity of the power converter setup and control, this proposed sustainable energy generation system algorithm suggests a combined inverter-battery-based DFIG design for wind energy generation [9].

Besides the prediction of uncertainty associated with wind energy, its cyclical fluctuation and irregular nature will make it a difficult attempt, especially for supplying isolated loads. Thus, the investigators suggested combining solar and wind energy to increase efficiency and also to maintain supply continuity for users residing in isolated areas. As far as we are aware, the majority of the work on hybrid wind-solar photovoltaic (SPV) systems has utilized permanent magnet generators and squirrel-cage induction generators for wind energy [10], [11]. Thus, this research work aims to investigate the performance of wind-driven DFIG in combination with an SPV system for stand-alone purposes. A model of the suggested design for stand-alone operations has been constructed, and its functionality has been tested extensively. The next sections describe the details regarding the proposed system structure, the creation of closed-loop control approaches, and conclusions drawn from the experimental investigations [12], [13].

Additionally, DFIG in the suggested system contains two voltage source converters (VSC). Along with the grid side converter (GSC), DFIG incorporates another VSC into the rotor circuit, referred to as the rotor side converter (RSC). The purpose of RSC is to attain wind maximum power point tracking (MPPT). The SPV system is attached to the DC bus via a solar converter, which enhances the voltage of the solar photovoltaic array. Solar energy can be evacuated efficiently and economically using this configuration. Additionally, this converter incorporates a solar MPPT control approach to optimize solar energy harvesting. In the absence of a wind energy source and a battery with a low level of charge, the battery bank could be recharged using grid electricity or a diesel generator connected to the same RSC. The GSC assists in maintaining the specified voltage and frequency at the output terminal in certain circumstances, such as inadequate solar or wind energy and variation in the quantity of solar and wind energy. Disruption of the distribution network due to a load loss or failure and loads of various forms, such as nonlinear and unbalanced loads. The key contributions of this research are as follows:

- To combine a DFIG and SPV system, an extensive adaptive performance evaluation of stand-alone or grid-tied HSEGS is conducted.
- To use the optimal torque wind MPPT method to improve wind energy harvesting with respect to wind turbine (WT) speed characteristics.

- The hybrid particle swarm optimization-perturb and observe (PSO-P&O) MPPT method is employed to maximize the power output from a solar PV system.
- The bidirectional converter control aims at extracting the maximum power from the SPV array while controlling the current via ESS.
- The presented technique is examined for various types of nonlinear, linear, and dynamic loads in different climatic conditions and the complete control scheme ensures that customers get reliable power in all conditions.

2. PROPOSED WIND SOLAR HYBRID MODEL

The suggested hybrid sustainable energy generating system (HSEGS)-linked micro-grid is represented in Figure 1. A similar system is developed for locations with peak power requirements of 5 kW and average power requirements of 2.5 kW, respectively. In HSEGS, the estimated capacity of both solar and wind energy units is considered to be 5 kW. A capacity utilization rate of 15% to 20% is assumed for both energy units, which is sufficient to meet the full-day energy demands of isolated villages. The battery bank is attached to the DC side of the RSC and GSC. RSC supports the wind energy system is operating at the optimal rotational speed specified by the wind MPPT (W_{MPPT}) technique. The GSC regulates the frequency and voltage of the network.

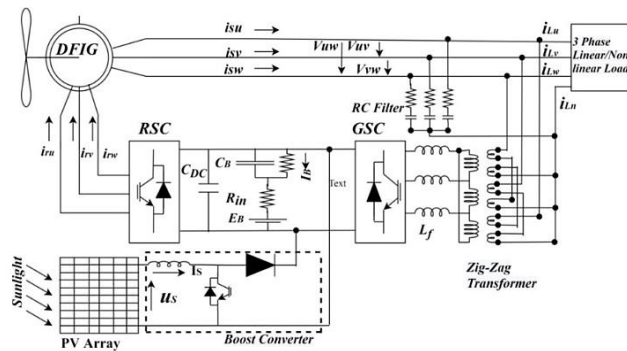


Figure 1. Overview of solar-wind hybrid sustainable energy generating system

2.1. Modelling of wind turbine

The wind turbine (WT) collects the kinetic energy from the wind and is used to provide operating torque to DFIG. The formula for extracted mechanical power (PM) is represented in view of the power capture coefficient. C_p and wind velocity v_w are defined as (1) [14].

$$P_M = 0.5\pi C_p \rho r^2 v_w^3 \quad (1)$$

Where, v_w , r , C_p , β , ρ , and λ are wind velocity, blade radius, power coefficient, pitch angle of blade air density, and tip speed ratio respectively. In addition, the coefficient of the captured C_p is a nonlinear form of β and λ , that can be represented as:

$$C_p(\lambda, \beta) = 0.73 \times \left(\frac{151}{\lambda_i} - 0.0023^{2.14} - 13.2 \right) \times e^{-\left(\frac{18.4}{\lambda_i} \right)} \quad (2)$$

and

$$\zeta_i = \left[\frac{1}{(\lambda + (\beta \times 0.080))} \right] \left[\frac{0.0350}{(\beta^3 + 1)} \right] \quad (3)$$

here, β and λ is the blade pitch angle and tip-speed ratio.

$$\lambda = \left(\frac{\omega_r \times r}{\eta_{GR} \times v_w} \right) \quad (4)$$

Tip speed ratio (TSR) is associated with the wind velocity v_w , turbine radius r and speed ω_r and η_{GR} is the turbine shaft gear ratio as (5).

$$\eta_{GR} = \left(\frac{\omega_{mr} \times r}{\lambda \times v_{rw}} \right) \quad (5)$$

The wind generator employed in the suggested strategy has a rated capacity of 4 kW at an operating wind speed (V_{rw}) of 9.0 m/s and a rotational speed (ω_{mr}) of 98.0 rad/s. Turbine radius and TSR (λ^*) is set to 4.3 m and 5.67 m respectively. The control operation keeps WMPPT until the machine attains the required speed (ω_{mr}), then the turbine shift gear ratio is 16.67.

To achieve a changeable frequency supply, back-to-back (BTB) converters are interconnected via the DC link between the DFIG's grid and rotor. Voltage-source converters equipped with bidirectional switches are employed. Each converter is composed of three legs, each of which links to one of the 3 ϕ system. The GSC's primary aim is to manage the reactive power absorbed by the DFIG's rotor in order to generate the rotor flux and maintain the system's continuous DC bus voltage, as illustrated in Figure 2 [15], [16].

The RSC primary objectives are to inject 3 ϕ voltage into the rotor at slip frequency, to keep the stator power factor, and to optimize DFIG power with the use of the MPPT technique, as illustrated in Figure 3. Since these converters are involved in bi-directional power flows in the system, they are liable for the power. To generate the specified frequency and voltage, as well as to control the reactive power flow in the system, it is essential to have control over these converters. As a result, the GSC and RSC are regulated via stator flux-oriented control. Both the rotor and stator rotational frames are transformed to d-q axis frames using this controller approach, which rotates at a synchronous frequency (ω_s) [17], [18] as illustrated in Figure 2.

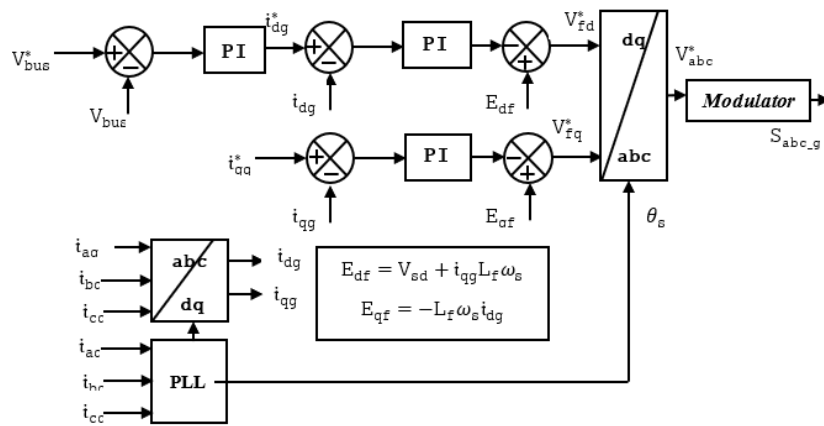


Figure 2. Grid-side controllers using vector control

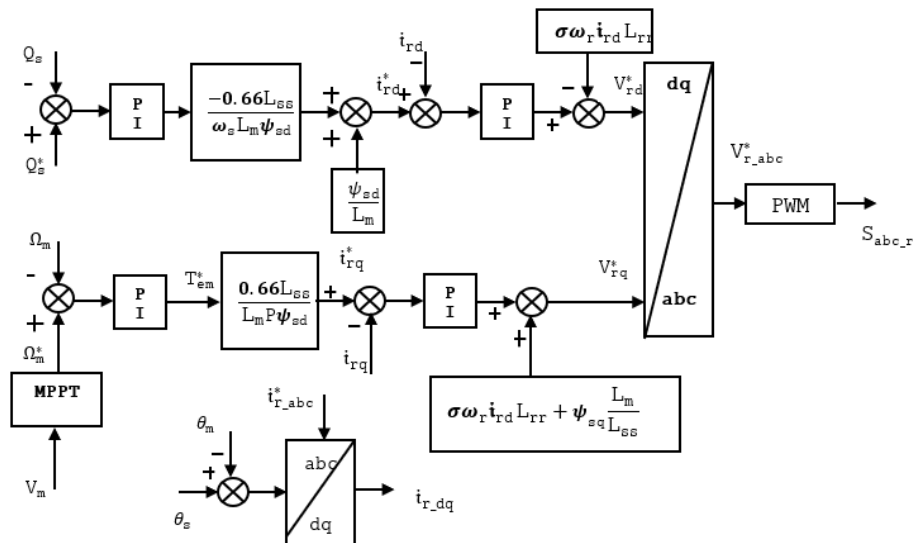


Figure 3. Rotor-side controllers using vector control

Without taking into account the saturation, impact the d-q terminal voltage can be expressed as:

$$V_{sd} = i_{sd}R_s + \frac{d\psi_{sd}}{dt} - \omega_s\psi_{sq} \quad (6)$$

$$V_{sq} = i_{sq}R_s + \frac{d\psi_{sq}}{dt} - \omega_s\psi_{sd} \quad (7)$$

$$V_{rd} = i_{rd}R_r + \frac{d\psi_{rd}}{dt} - \omega_r\psi_{rq} \quad (8)$$

$$V_{rq} = i_{rq}R_r + \frac{d\psi_{rq}}{dt} - \omega_r\psi_{rd} \quad (9)$$

the equations of flux coupling:

$$\psi_{sd} = i_{sd}L_{ss} + L_m i_{rd} \quad (10)$$

$$\psi_{sq} = i_{sq}L_{ss} + L_m i_{rq} \quad (11)$$

$$\psi_{rd} = i_{sd}L_m + L_{rr}i_{rd} \quad (12)$$

$$\psi_{rq} = i_{sq}L_m + L_{rr}i_{rq} \quad (13)$$

where, $L_{ss} = L_s + L_m$ & $L_{rr} = L_r + L_m$. Torque equation can be expressed as (14).

$$T_g = 1.5(i_{rd}\psi_{sq} - i_{sd}\psi_{rd})P \frac{L_m}{L_s} \quad (14)$$

Active and reactive powers of a stator are as follows:

$$P_s = 1.5(i_{rd}V_{rd} + i_{sd}V_{sd} + i_{sq}V_{sq} + i_{rq}V_{rq}) \quad (15)$$

$$Q_s = 1.5(i_{sq}V_{sd} + i_{sd}V_{sq} - i_{rq}V_{rd} + i_{rd}V_{rq}) \quad (16)$$

2.2. Calculation of DFIG rating

DFIG, the extrinsic power supply passes via the stator and rotor. Without regard for losses, the minimal power of a DFIG (P_E) is proportional to the specified air gap power (P_{AIR_G}), at maximal wind velocity, defined as (17).

$$P_E = \left(\frac{P_{AIR_G}}{1 + |S_{P_MAX}|} \right) \quad (17)$$

Where, S_{P_MAX} is the slip coefficient associated with the turbine velocity, ω_{mr} has -0.268. The velocity range of DFIG correlates to the velocity range of slip 0.3 to -0.268. Consider the air gap power (P_{AIR_G}) is equivalent to the mechanical input power, DFIG power rating matches the maximal input power, is $\cong 3$ kW. The WT is operating; RSC supplies the machine with its entire magnetizing power demands. As a result, the 3-kW capacity of the DFIG is sufficient to transform mechanical power by 4 kW WT into electrical power.

2.3. Battery sizing

The DFIG has an optimum working slip of 0.3 and 110 rad/s, in which the speed is associated with this slip. At this point, the rotor maximal line voltage (V_{R_max}) can be expressed as (18).

$$V_{R_max} = (415 * 0.3) = 124.5V \quad (18)$$

PWM controlling requires the appropriate DC bus voltage (V_{B_DC}) and it is expressed as (19).

$$V_{B_DC} > \left[\frac{(1.632 \times V_{LL})}{e_i} \right] \quad (19)$$

V_{LL} equals the difference between the line voltage on the zig-zag transformer LV sides and the rotor voltage at optimum slip. The optimum working slip is 0.3. As a result, maximal rotor voltage and the zig-zag

transformer LV side is 125 V. The e_i is set to unity as the modulation index. The V_{B_DC} necessary for the operation of PWM control should not be lesser than 204 kV dependent on such inputs. V_{B_DC} is considered to be 240 kV in the suggested technique.

The suggested hybrid system is intended to meet average load requirements of 2.5 kW up to 24 hours without the need for any generating device. By adding 20% leeway for energy losses throughout energy transfer, the needed battery storage capacity increases to 72 kWh. The batteries AH capacity increases to 300 Ah, when the $V_{B_DC} = 240$ kV. This is accomplished by dividing 20 numbers of 12 V, 360 Ah lead-acid battery uniformly into 2 parallel networks.

2.4. Modeling of photovoltaic array

The photovoltaic module delivers the following current as (20).

$$I = (I_{PH}N_P - I_0N_P) \times \left[\exp \left(\frac{\frac{V}{N_S} + \frac{R_S}{N_P} \times I}{V_T n} - \frac{1}{T} - \frac{1}{T_R} \right) - 1 \right] - I_{SH} \quad (20)$$

Where, V_T : thermal voltage of diode (V), N_P : the total number of cells that are interconnected in parallel, R_{SH} : shunt resistance, and R_S : series resistance respectively. Solar panels are designed in such a way that their open circuit voltage keeps lesser than V_{B_DC} . The number of cells in a series is proportional to the DC voltage V_{B_DC} and V_{C_OCV} voltage across the open circuit of a cell as (21).

$$N_C = \frac{V_{B_DC}}{V_{C_OCV}} \quad (21)$$

V_{C_OCV} is taken to be 0.696 V, depending on the properties and value of a standard commercially available cell. 216 V is the minimal voltage of lead-acid battery. Because of tolerances during manufacture in electrical modules, the panel voltage might vary by up to $\pm 3\%$. Thus, V_{B_DC} is considered to be 209.5 V, and needed number of cells, N_C , is $\cong 300$ cells as determined from (21). To ensure that the cells are distributed uniformly in a conventional design, 301 cells are chosen and divided into 5 units of 60 cells each. For a standard unit characteristic, the ratio of V_{C_OCV} to cell voltage at maximal power point (MPP), V_{MPP} is 0.659 V. Consequently, the device voltage at MPP is 39.54 V. At a capacity of 4 kW, an overall module current at MPP is 20.23 A. Table 1 contains the detailed specifications for DFIG system and Table 2 contains the implementation parameters which are required to design the solar energy unit.

Table 1. DFIG specifications

Parameters	Value	Parameters	Value
P_{rated}	3.0 kW	Pole pairs	2
V_{stator}	400 V	R_s	1.342 Ω
Rotor shaft speed	1500 RPM	R_r	1.71 Ω
Operating frequency	50 Hz	L_r	83.42 mH
I_s	12 A	L_m	218 mH
J	0.1876 kg m^2		

Table 2. Technical parameters of solar energy unit

Parameter	Value	Parameter	Value
PV model rating	266.6 Wp	V_{MPP} of PV panel	39.54 V
N_s	5	Total current of PV string	20.23 A
N_p	3	I_{MPP} of PV panel	6.743 A
V_{C_OCV} of PV cell	0.696 V	PV module I_{sc}	7.819 A
V_{MPP} of PV cell	0.659 V		

3. HYBRID SUSTAINABLE ENERGY GENERATING ALGORITHM

Three blocks constitute the control of HSEGS: the RSC block, the GSC block, and the DC-DC converter block. These blocks are described below.

3.1. Proposed hybrid PSO-P&O MPPT technique

Figures 4(a) and 4(b) (see Appendix) display the proposed H-MPPT algorithm flowchart. The algorithm maintains the operating point at the MPP using P&O until it detects a partial shadow. When the tracking is complete, the MPP data is recorded, which includes peak power, current, and voltage. It then compares the present current and voltage to the most recent data to determine partial shading. When partial shading is detected, the approach determines whether the initial peak (the rightmost) is the global peak or not. If the power differential criteria is reached, the present MPP is considered effective; otherwise, the "main-program" identifies the need to track the MPP and launches the "MP-track sub-program" [19].

In the "MP-track sub-program," the appropriate voltage range is chosen. The PSO scans this region and provides the higher Pi value. The need for tracking future peaks is considered. If the power discrepancy criterion is met, the GMPP value is determined by comparing each of the recorded MPP power values. If the requirement fails, a similar step is repeated until all peaks are considered. When the "MP-track sub-program" returns, the P&O approach maintains the operating point at the MPP.

3.2. DFIG wind turbine MPPT

The primary goal of a WT working in region 2 of its speed attributes is to harvest the maximum amount of wind energy possible from the wind through the use of MPPT. It can be calculated by using either the actual wind velocity as a reference for the controllers or the torque as a reference [20]-[24]. The optimal torque (OT) method proposes the controller which is a control method that employs a proportional plus integral controller to regulate the wind WTs torque, which is proportional to the WTs square of its angular momentum. Unlike, the TSR method, this approach does not require an anemometer to measure wind velocity since these readings are inefficient, time-consuming, and inaccurate. This method primary goal is to assess the optimal operating point without relying on wind speed observations [25]. At optimum power point:

$$\lambda_{OPT} = \frac{\Omega_t R}{u} \quad (22)$$

$$C_P = C_{PMAX}, C_T = C_{TOPT} \quad (23)$$

obtain the best TSR value by (27) it to the torque derived from the turbine equation.

$$T_T = 0.5\pi\rho R^3 C_T \times \left(\frac{\Omega_t R}{\lambda_{OPT}}\right)^2 \quad (24)$$

$$T_T = \frac{0.5\pi\rho R^3 C_{PMAX}}{\lambda_{OPT}} \times \left(\frac{\Omega_t^2 R^2}{\lambda_{OPT}^2}\right) \quad (25)$$

$$T_T = \frac{0.5\pi\rho R^5 C_{PMAX} \Omega_t^2}{\lambda_{OPT}^3} \quad (26)$$

$$T_T = K_{OPT} \times \Omega_t^2 \quad (27)$$

The OT value with TOPT is used as the reference torque and it is contrasted to the current torque value. The discrepancy between these torque values are interpreted by the PI controller as an error signal. This controller feeds back the revised torque value to minimize error signals, as illustrated in Figure 4(c) (see Appendix). This is the quickest and most efficient technique for determining the wind turbine's optimum operational power point as no wind observation is required.

4. RESULTS AND DISCUSSION

MATLAB is employed to develop the Simulink model of the HSEGS-fed microgrid. Wind turbines and solar panels are modeled based on their operational characteristics. The HSEGS effectiveness under various wind speeds and sun irradiation conditions is illustrated in Figures 5 and 6. Both of the preceding scenarios also examine the MPPT in the presence of changing wind speeds and radiation levels via a solar converter and RSC. Additionally, the effectiveness of SEGS is examined with different electrical loads, including balanced and unbalanced linear loads (Figures 7 and 8). The modeling and simulation of HSEGS were conducted utilizing the specified variables and their values.

4.1. HSEGS effectiveness under variable solar radiation conditions with fixed wind speeds and load

Figure 5 illustrates the effectiveness of an HSEGS with different solar irradiation and constant wind speeds. The device is operating at 7 m/s wind speed and 700 W/m² global sun irradiance. At t = 4.0 s, the solar irradiance is raised to 800 W/m² at a level of 400 W/m² and then dropped to 700 W/m² at the same level, beginning at t = 5.25 s. Once again, it is determined that the device is capable of supplying the specified voltage and frequency when operated at the MPPT of the solar PV panel.

4.2. HSEGS effectiveness under various wind conditions with fixed solar radiation and load

Figure 6 represents the outcome of HSEGS with continuous solar irradiation and fluctuating wind. The device is started with a 7 m/s wind speed. The solar radiation is maintained at 800 W/m² throughout the simulation time. The load terminals are connected to three-phase balanced loads of 2.5 kW and 1 kVAR. The generator speed increases to 153 rad/s when the wind speed is increased. At 4.0 s, the wind speed is increased to 7.5 m/s, and the matching generator benchmark speed is raised to 164 rad/s. At 7.25 s, the wind speed decreases to 6.5 m/s while maintaining the same pace of shift. As illustrated in Figure 6, even when the turbine and generator powers are mismatched in the device, the voltage and frequency remain unchanged despite variations in wind speed.

4.3. HSEGS effectiveness in non-linear and unbalanced load

The system efficiency for non-linear and unbalanced loads is demonstrated in Figure 7. The device is initiated with a balanced load of 4.0 kW that consists of linear and nonlinear loads. The first phase 'U' is opened at $t = 4.60$ s and the V phase is disconnected at $t = 4.80$ s, then creates 1ϕ -load. It has been noticed that the device can produce a rated frequency and voltage in both scenarios. Total harmonic distortion (THD) value is less than 3.6% in both circumstances - with no exceptions.

4.4. HSEGS effectiveness in dynamic loads

The system efficiency at dynamic load is demonstrated in Figure 8. In contrast, non-linear and dynamic loads, including pumps and compressors, are also typical and must be accommodated by the DG system. Considering half of the overall load demand is expected to be 3.0 kW, the motor load should be limited, i.e., 2 HP = 1.4914 kW. The efficiency of the HSEGS with the motor taken in operation at $t = 3.34$ s and the load torque applied as per the axial pump. It has been demonstrated that GSC is capable of supplying the requisite reactive power to a device without disrupting the system voltage.

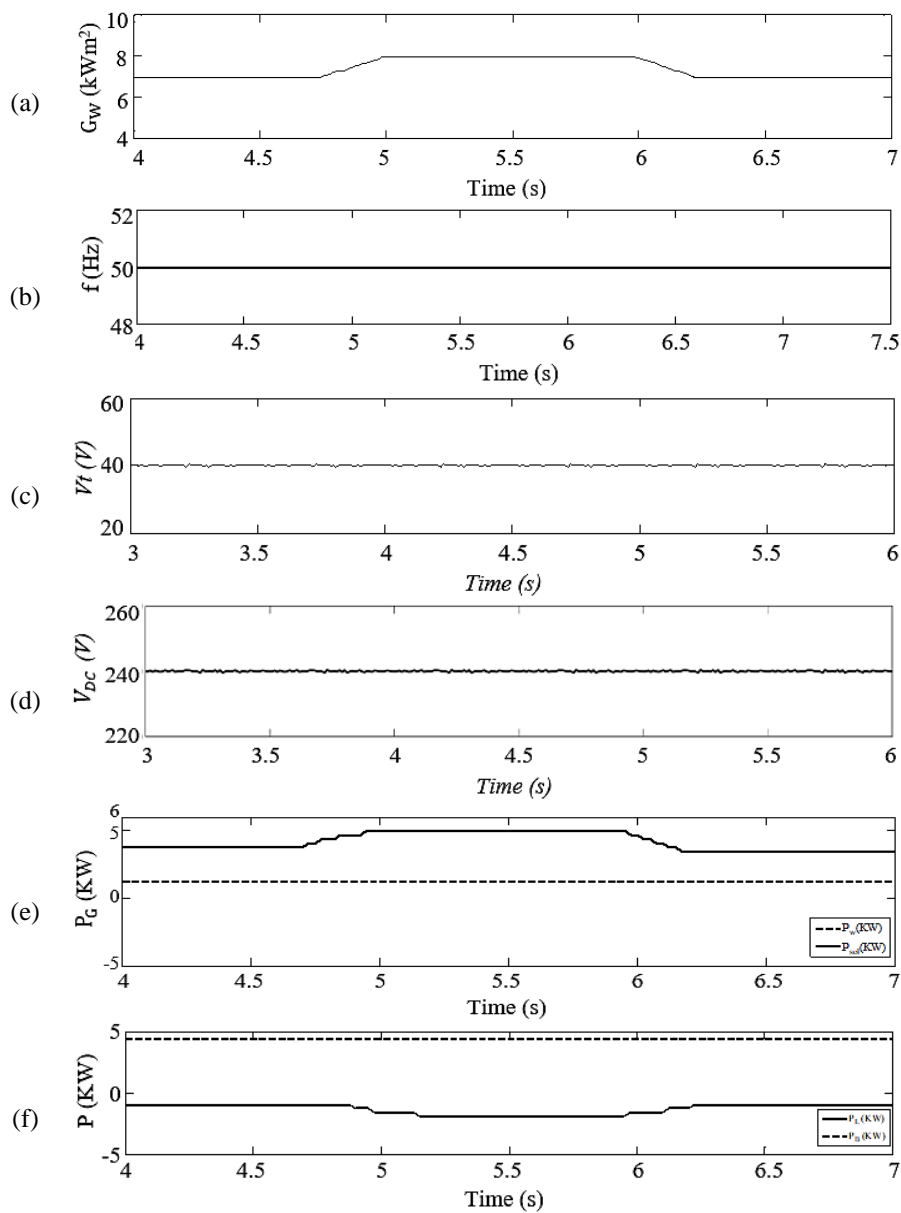


Figure 5. HSEGS effectiveness at variable solar irradiance: (a) solar irradiances, (b) frequency of output voltage, (c) terminal voltage, (d) DC bus voltage, (e) solar and wind power generation, and (f) load and battery power

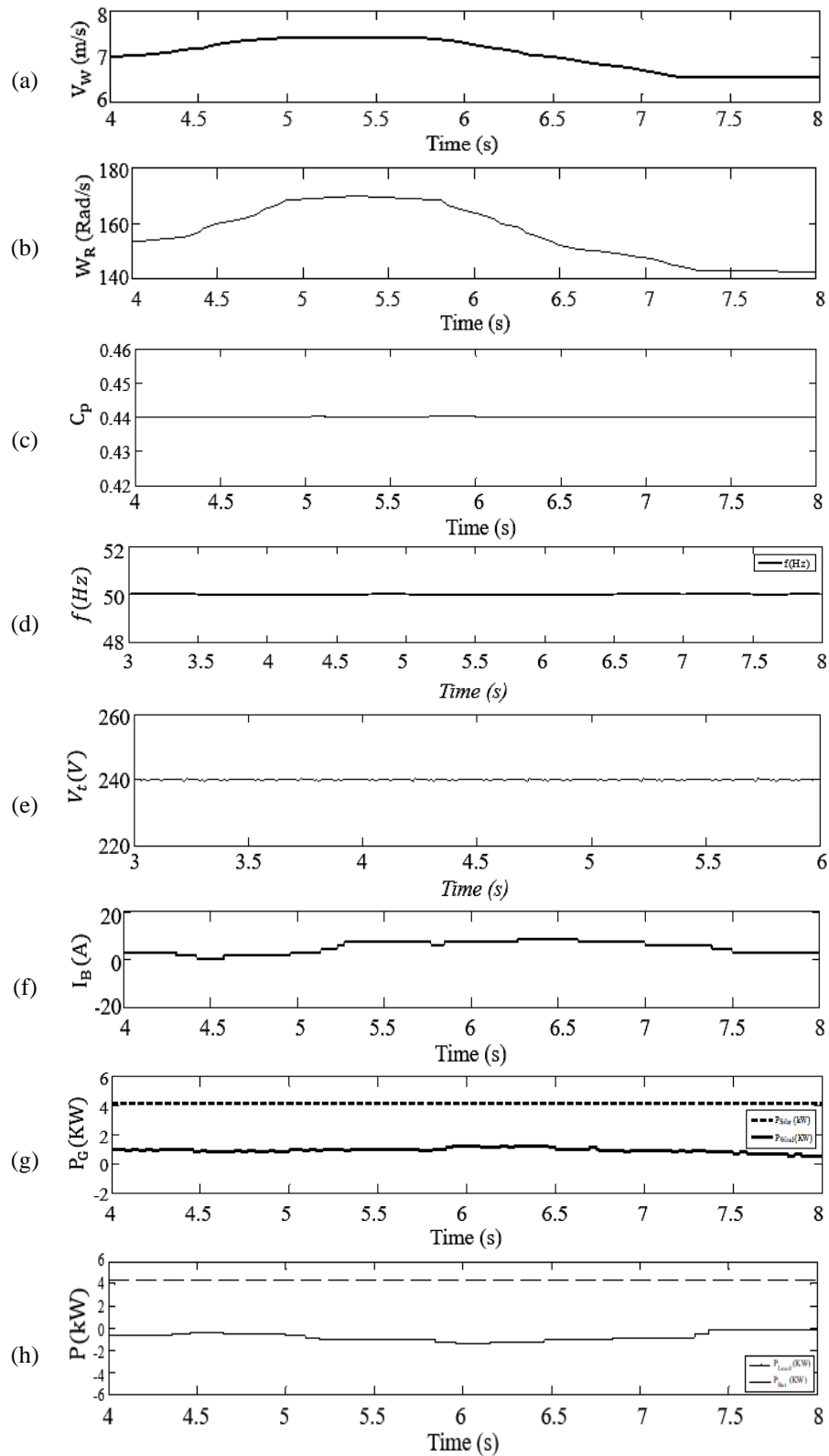


Figure 6. HSEGS effectiveness under various wind conditions: (a) wind speed, (b) wind speed in radians, (c) power capture coefficient, (d) frequency of output voltage, (e) terminal voltage, (f) battery current, (g) solar and wind power generation, and (h) load and battery power

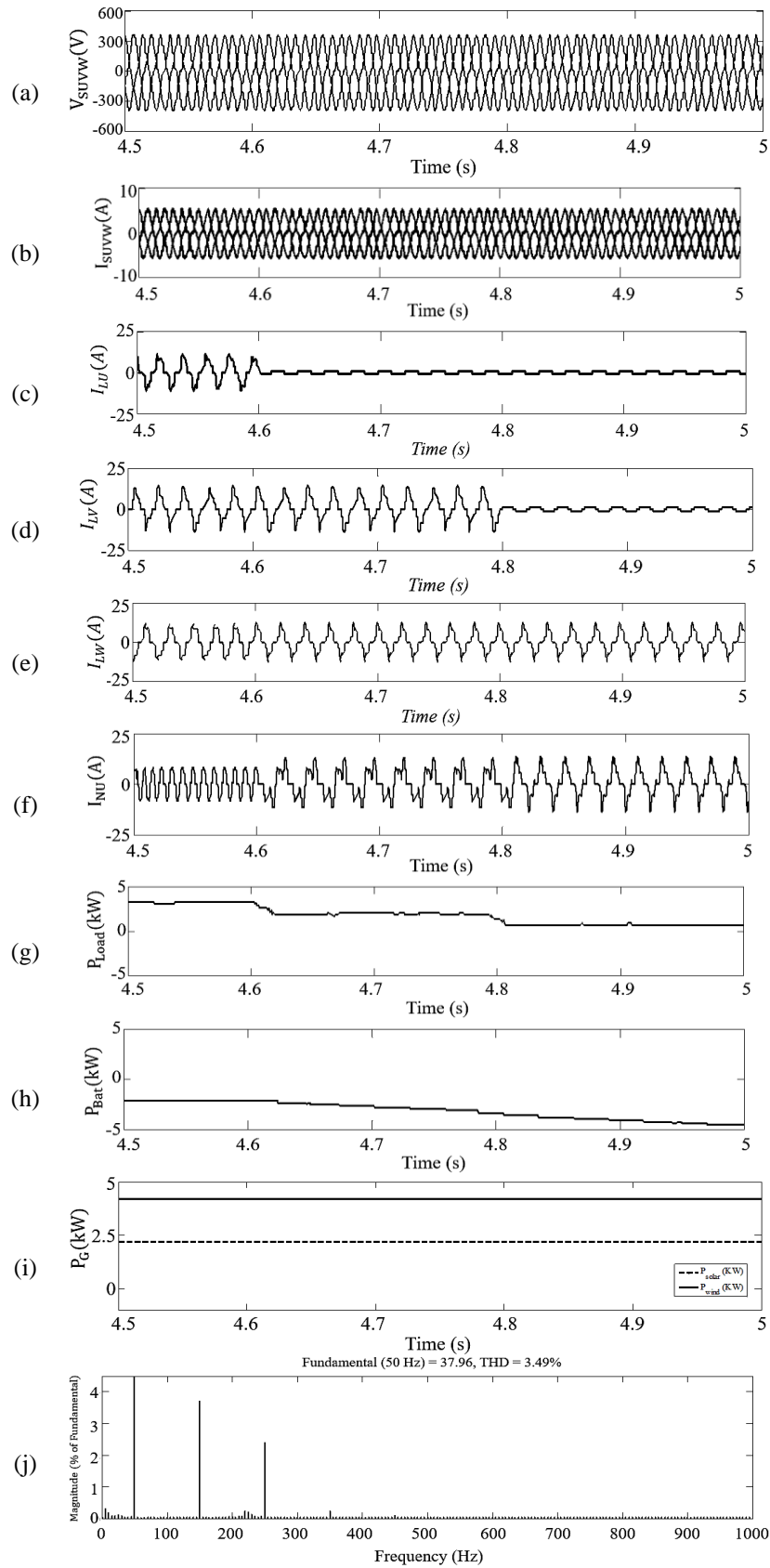


Figure 7. HSEGS effectiveness in non-linear and unbalanced load: (a) stator voltage, (b) stator current, (c) U phase load current, (d) V phase load current, (e) W phase load current, (f) neutral load current, (g) load power, (h) battery power, (i) solar, and wind power generation, and (j) THD

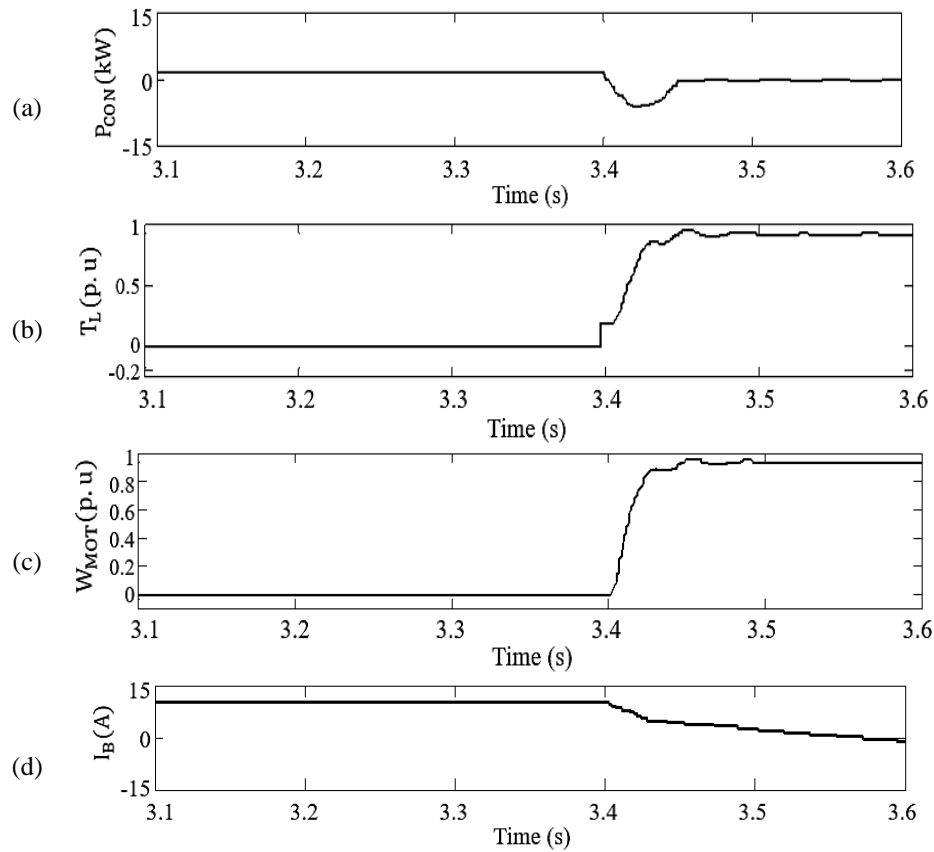


Figure 8. HSEGS effectiveness in dynamic loads: (a) stator current, (b) load torque, (c) motor power, and (d) battery current

5. CONCLUSION

The wind and solar energy are free; they are unpredictable and have a significant degree of fluctuation. These renewable energy sources can be constructed more customer-pleasantly through the use of power storage and smart PE control. This research discusses the analytical and empirical validation of an HSEGS comprised of a wind turbine with DFIG and a photovoltaic array. Both solar and wind energy units incorporate MPPT logic to optimize energy extraction while also enhancing the total efficiency of the system. The results of simulations on a standalone SPV system employing P&O-MPPT evidently show that the technique is more efficient than IC-MPPT techniques. The HSEGS is modeled in MATLAB Simulink and controls and optimizes output power employing TSR and OT-MPPT techniques. The result of HSEGS shows that the optimal torque technique has superior dynamic behavior to wind speed fluctuation when contrasted to the TSR technique. Additionally, it is determined that the power quality is in an appropriate range. The suggested HSEGS has been proven to work well under a variety of electrical and mechanical dynamic scenarios. Under a variety of dynamic scenarios, the HSEGS demonstrated the capability to track optimum power, compensate for neutral current, eliminate harmonics, and balance the load, in addition to regulating the system frequency and voltage. This enhances the system's importance for distributed generation in isolated regions, allowing residents to meet their energy needs without relying on the external grid.

APPENDIX

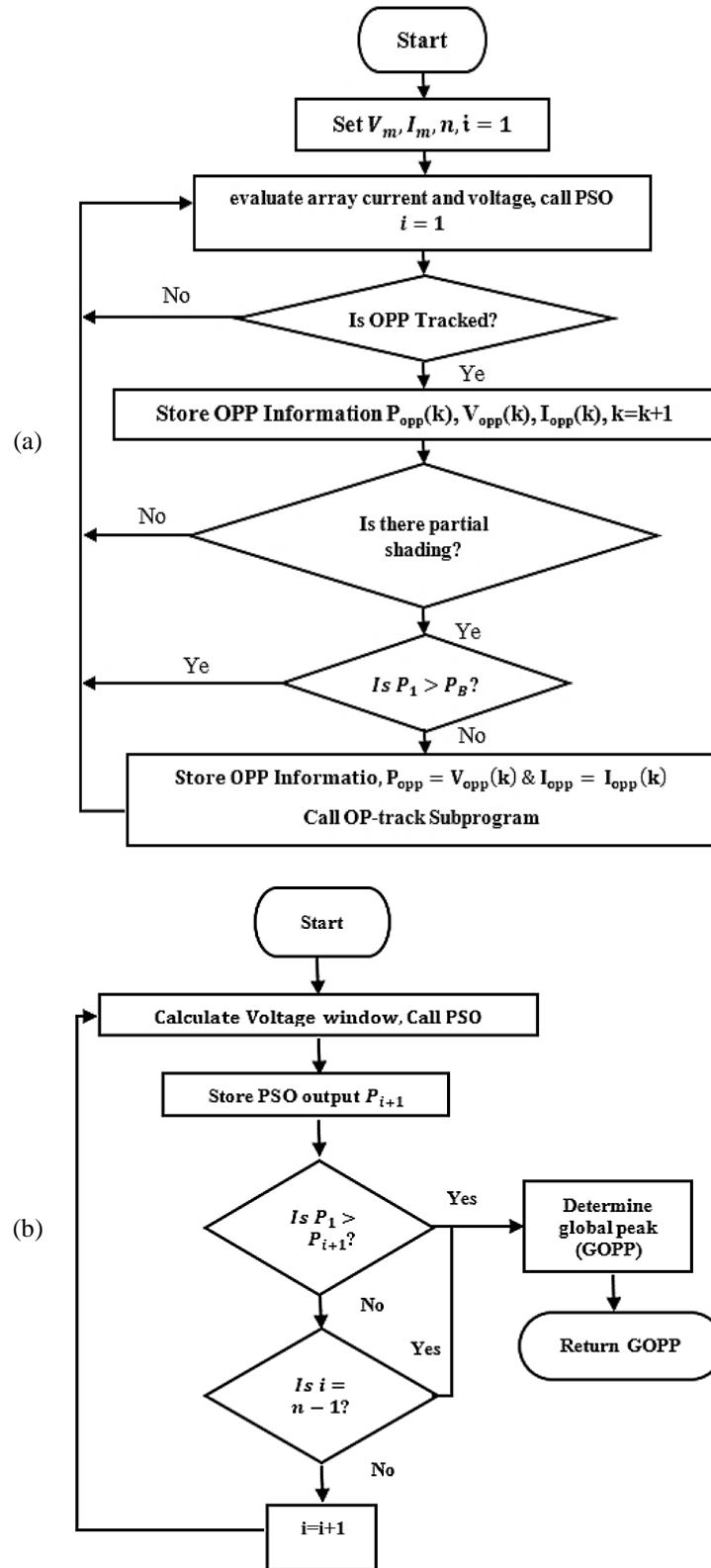


Figure 4. Flowcharts for the suggested hybrid PSO-P&O MPPT method:
(a) main program and (b) OP-track sub-program

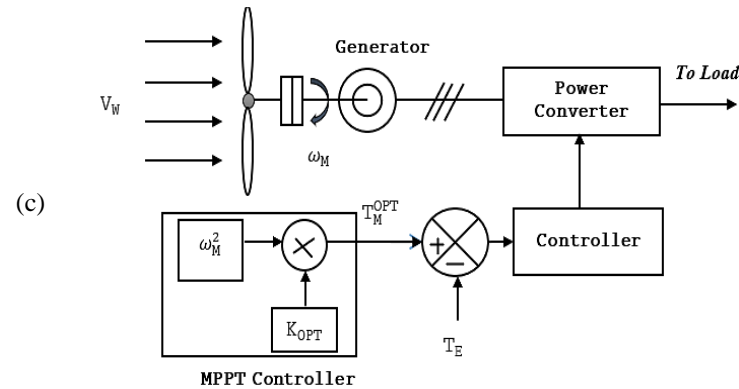


Figure 4. Flowcharts for the suggested hybrid PSO-P&O MPPT method:
(c) MPPT technique with an OT of the wind velocity curve (continued)




REFERENCES

- [1] Y. Kebbati and L. Baghli, "Design, modeling, and control of a hybrid grid-connected photovoltaic-wind system for the region of Adrar, Algeria," *International Journal of Environmental Science and Technology*, vol. 20, no. 6, pp. 6531–6558, Jun. 2023, doi: 10.1007/s13762-022-04426-y.
- [2] D.-A. Ciupăgeanu, G. Lăzăroiu, and L. Barelli, "Wind energy integration: Variability analysis and power system impact assessment," *Energy*, vol. 185, pp. 1183–1196, Oct. 2019, doi: 10.1016/j.energy.2019.07.136.
- [3] D.-A. Ciupăgeanu, L. Barelli, and G. Lăzăroiu, "Real-time stochastic power management strategies in hybrid renewable energy systems: A review of key applications and perspectives," *Electric Power Systems Research*, vol. 187, p. 106497, Oct. 2020, doi: 10.1016/j.epsr.2020.106497.
- [4] A. Mahesh and K. S. Sandhu, "Hybrid wind/photovoltaic energy system developments: Critical review and findings," *Renewable and Sustainable Energy Reviews*, vol. 52, pp. 1135–1147, Dec. 2015, doi: 10.1016/j.rser.2015.08.008.
- [5] A. Kumar, Shivashankar, and B. S. Ram, "Efficient solar integrated doubly fed induction generator for wind energy harnessing," *Recent Advances in Electrical & Electronic Engineering (Formerly Recent Patents on Electrical & Electronic Engineering)*, vol. 13, no. 5, pp. 723–735, Sep. 2020, doi: 10.2174/2352096512666191019094707.
- [6] G. B. A. Kumar and Shivashankar, "Optimal power point tracking of solar and wind energy in a hybrid wind solar energy system," *International Journal of Energy and Environmental Engineering*, vol. 13, no. 1, pp. 77–103, Mar. 2022, doi: 10.1007/s40095-021-00399-9.
- [7] A. M. Hemeida *et al.*, "Optimum design of hybrid wind/PV energy system for remote area," *Ain Shams Engineering Journal*, vol. 11, no. 1, pp. 11–23, Mar. 2020, doi: 10.1016/j.asej.2019.08.005.
- [8] J. F. Manwell, "Hybrid Energy Systems," *Encyclopedia of Energy*, vol. 3, pp. 215–229, 2004.
- [9] B. M. K. Kumar, S. N. Rao, and M. S. Indira, "Analysis of grid-connected reduced switch MLI with high-gain interleaved boost converter and hybrid MPPT for solar PV," *International Journal of Energy and Environmental Engineering*, vol. 13, no. 4, pp. 1287–1307, Dec. 2022, doi: 10.1007/s40095-022-00479-4.
- [10] A. Goswami, P. Sadhu, and P. K. Sadhu, "Development of a grid connected solar-wind hybrid system with reduction in levelized tariff for a remote island in India," *Journal of Solar Energy Engineering*, vol. 142, no. 4, p. 044501, Aug. 2020, doi: 10.1115/1.4046147.
- [11] S. Aggarwal, "Power markets in transition: consequences of oversupply and options for market operators," *Current Sustainable Renewable Energy Report*, vol. 6, pp. 29–33, 2019, doi: 10.1007/s40518-019-00123-6.
- [12] G. S. Kaloi, J. Wang, and M. H. Baloch, "Active and reactive power control of the doubly fed induction generator based on wind energy conversion system," *Energy Reports*, vol. 2, pp. 194–200, Nov. 2016, doi: 10.1016/j.egy.2016.08.001.
- [13] S. Rehman, "Hybrid power systems – sizes, efficiencies, and economics," *Energy Exploration & Exploitation*, vol. 39, no. 1, pp. 3–43, Jan. 2021, doi: 10.1177/0144598720965022.
- [14] B. Bhandari, S. R. Poudel, K.-T. Lee, and S.-H. Ahn, "Mathematical modeling of hybrid renewable energy system: A review on small hydro-solar-wind power generation," *International Journal of Precision Engineering and Manufacturing-Green Technology*, vol. 1, no. 2, pp. 157–173, Apr. 2014, doi: 10.1007/s40684-014-0021-4.
- [15] A. Acakpovi, P. Adjei, N. Nwulu, and N. Y. Asabere, "Optimal hybrid renewable energy system: a comparative study of wind/hydrogen/fuel-cell and wind/battery storage," *Journal of Electrical and Computer Engineering*, vol. 2020, pp. 1–15, Dec. 2020, doi: 10.1155/2020/1756503.
- [16] R. Zhu, A. Zhao, G. Wang, X. Xia, and Y. Yang, "An energy storage performance improvement model for grid-connected wind-solar hybrid energy storage system," *Computational Intelligence and Neuroscience*, vol. 2020, pp. 1–10, Aug. 2020, doi: 10.1155/2020/8887227.
- [17] M. K. Bourdoulis and A. T. Alexandridis, "PI control design and passivity/stability analysis for DFIG wind systems under vector control constraints," 2012, doi: 10.2316/P.2012.781-035.
- [18] S. Karad and R. Thakur, "Recent trends of control strategies for doubly fed induction generator based wind turbine systems: A comparative review," *Archives of Computational Methods in Engineering*, vol. 28, no. 1, pp. 15–29, Jan. 2021, doi: 10.1007/s11831-019-09367-3.
- [19] M. A. Soliman, H. M. Hasanien, and A. Alkuhayli, "Marine predators algorithm for parameters identification of triple-diode photovoltaic models," *IEEE Access*, vol. 8, pp. 155832–155842, 2020, doi: 10.1109/ACCESS.2020.3019244.
- [20] A. O. Baba, G. Liu, and X. Chen, "Classification and evaluation review of maximum power point tracking methods," *Sustainable Futures*, vol. 2, p. 100020, 2020, doi: 10.1016/j.sfr.2020.100020.




- [21] B. Pakkiraiah and G. D. Sukumar, "Research survey on various MPPT performance issues to improve the solar PV system efficiency," *Journal of Solar Energy*, vol. 2016, pp. 1–20, Jul. 2016, doi: 10.1155/2016/8012432.
- [22] M. Kamran, M. Mudassar, M. R. Fazal, M. U. Asghar, M. Bilal, and R. Asghar, "Implementation of improved Perturb & Observe MPPT technique with confined search space for standalone photovoltaic system," *Journal of King Saud University - Engineering Sciences*, vol. 32, no. 7, pp. 432–441, Nov. 2020, doi: 10.1016/j.jksues.2018.04.006.
- [23] H. H. H. Mousa, A.-R. Youssef, and E. E. M. Mohamed, "Hybrid and adaptive sectors P&O MPPT algorithm based wind generation system," *Renewable Energy*, vol. 145, pp. 1412–1429, Jan. 2020, doi: 10.1016/j.renene.2019.06.078.
- [24] İ. Yazıcı and E. K. Yaylacı, "Improving Efficiency of the tip speed ratio-MPPT method for wind energy systems by using an integral sliding mode voltage regulator," *Journal of Energy Resources Technology*, vol. 140, no. 5, p. 051203, May 2018, doi: 10.1115/1.4038485.
- [25] D. Song, J. Yang, M. Su, A. Liu, Y. Liu, and Y. Joo, "A comparison study between two MPPT control methods for a large variable-speed wind turbine under different wind speed characteristics," *Energies*, vol. 10, no. 5, p. 613, May 2017, doi: 10.3390/en10050613.

BIOGRAPHIES OF AUTHORS






Dr. G. B. Arjun Kumar    has six patent and published more than 30 technical papers related to the domains wind energy, solar energy, hybrid energy, and power electronics in reputed international journals, and international/national conferences. Performed as a reviewer for journals including IET on Power Electronics and IEEE Access; and for many IEEE international conferences. Currently working as an Assistant Professor in the Department of Electrical and Electronics Engineering, Dayananda Sagar College of Engineering, Bangalore. He can be contacted at email: arjun-eee@dayanandasagar.edu.






Dr. M. Balamurugan    is currently working as an Assistant Professor in the Department of EEE, Dayananda Sagar College of Engineering, Bangalore. He was also awarded as best researcher in the year 2016 by VIT University. His research interests are cascaded multilevel inverter and power electronics applications in renewable energy systems. He has published several international papers in journals, book chapters, and conferences of high repute. He can be contacted at email: balamurugan-eee@dayanandasagar.edu.



Dr. K. N. Sunil Kumar    has a career spanning over twelve years in the field of industrial and engineering education. One patent and published more than 24 technical papers related to the domain of wireless communication, biomedical signal processing, IoT, and VLSI domain in reputed international journals, and international/national conferences. Currently working as a Professor in the Department of ISE, Sri Venkateshwara College of Engineering, Bangalore. He can be contacted at email: sunilkumarkn26@gmail.com.



Dr. Ravi Gatti    has a career spanning over nine years in the field of industrial and engineering education. He is the author of several articles published in international/national author bio(s) with photo(s) journals and conferences. Performed as a reviewer for journals including IET on Power Electronics and IEEE Access; and for many IEEE international conferences. His current interest includes wireless networks, scheduling algorithms in LTE-A systems, and the RRM process. He can be contacted at email: ravigatti-ece@dsatm.edu.in.